FUDMA Journal of Sciences (FJS)
ISSN online: 2616-1370
ISSN print: 2645 - 2944
Vol. 5 No. 2, June, 2021, pp 264-272
DOI: https://doi.org/10.33003/fjs-2021-0502-615

LAND SURFACE TEMPERATURE INVESTIGATION AROUND IKOGOSI WARM SPRING NIGERIA USING LANDSAT8 DATA

***[1]Bello, Y.A., [1]Lawal, K.M., [2]Dewu, B.B.M., and [3]Ikpokonte, A.E.**

[1]Physics Department, Ahmadu Bello, Zaria
[2]Center for Energy Research and Training, Ahmadu Bello University, Zaria
[3]Geology Department, Ahmadu Bello University, Zaria
Corresponding author's email: abuibraheem27@yahoo.com

ABSTRACT
Ikogosi warm spring (IWS) is among the most visited geothermal resource by tourists in Nigeria. On that basis, it has attracted so much attention from researchers using various geophysical methods, except the retrieval of the land surface temperature (LST) from remote sensing data. This work aimed at computing LST to delineate hot zone around Ikogosi geothermal resources. The split-window approach was used to compute the LST from Landsat 8 data. The interpretation of Landsat8 data revealed that the central region of the study area is of high LST, and the temperature then drops towards the southwest direction. The result also shows that the warm spring is situated around a region with high land surface temperature (about 29 °C) which is an indication of a geothermal reservoir. The supervised classification of the LST yields two zones of the high density of pixels with high temperature, hot spot zones. The hot spot zone west of IWS is believed to be the heat source of IWS as it has high LST, and it is closer to IWS while the hot spot zone NW of IWS shows an indication of a viable geothermal resource, high LST.

Keywords: Ikogosi warm spring, Land surface temperature, Emissivity, and heat source

INTRODUCTION

A heat source and fluid that transfer heat, through convection, towards the surface are essential in a geothermal system. The fluid that transfers the heat to the surface could be magma or water, and the heat source may be some kilometers away from the surface (Nicholson, 1993). If rising hot waters reach the surface then characteristic geothermal features such as hot springs, fumaroles, geysers, and mud pots may form (Heasler *et al*., 2009).

There are more than six geothermal resources in Nigeria in the form of hot springs of which the Ikogosi warm spring (IWS) is the most visited by tourists. A review of the geology of the study area is available in Bello *et al.* (2020). Several methods have been used to investigate IWS: Curie depths range from 5 to 16 km with shallow Curie depths region associated to magmatic intrusion at depth (Olorunfemi *et al.* 2011; Abraham *et al*. 2014), subsurface geological succession (Ojo *et al*. 2011), Radiometric investigation (Adegbuyi and Abimbola, 1997), and description of the origin of the water at depth, and the associated heat content from samples of water and rock at location (Adegbuyi *et al*., 1996). No published work has reported the computation of land surface temperature over IWS from remote sensing data (Landsat8).

Land surface temperature (LST) is useful in the detection of shallow geothermal anomalies by assessing remote sensing (Chan *et al.*, 2018). LST has been used as an indicator of volcanic complexes which are associated with thermal anomalies. LST from satellite data, such as Landsat8, gives an estimate of the kinetic temperature of the earth's surface skin (Norman & Becker, 1995),i.e., the aggregate surface medium viewed by the sensor to a depth of about 12 µm. This work aimed at the computation of LST retrieved from Landsat8 to delineate the hot zone around the Ikogosi geothermal resource.

MATERIAL AND METHOD

Ikogosi warm spring is known to discharge steady hot water and it is expected that the heat source is in the vicinity of the warm spring. The Landsat8 data covering the study area, figure 1 shows the dimension of the study area, was downloaded from the USGS website. The LST was computed to delineate regions of thermal anomalies. The data considered from remotely sensed data is Landsat8's red, near-infrared, and thermal infrared. The split-window algorithm was used to compute LST for the study area, the procedure is illustrated in figure 2 below.

First, thermal infrared remote sensor (TIRS) and operational land imager (OLI) bands were subjected to radiometric calibration to convert the Digital Number (DN) recorded by the remote sensor into the at-atmosphere radiance.

Equation 1 developed by the USGS was used to compute the spectral radiance from DN value of OLI and TIRS data of Landsat 8: The Thermals of band 10 and 11 and visible to shortwave infrared bands of 4 and 5 data stored as DN values were initially converted to spectral radiance values. The radiance factor necessary for the computation of the radiance for all bands are shown in table 1.

$L_\lambda = M_L\, Q_{cal} + A_L$ 1

L_λ = Spectral radiance ((W/(m^{2}srμm)).
M_L = Radiance multiplicative scaling factor for the band (RADIANCE_MULT_BAND_n from the metadata).
A_L = Radiance additive scaling factor for the band (RADIANCE_ADD_BAND_n from the metadata).
Q_{cal} = Level 1 pixel value in DN.
The scene calibration data are usually available on the metadata file of each Landsat scene. The following table (table 1) lists two sets of ML and AL for band 4, 5, 10 and 11 from metadata file of an image.

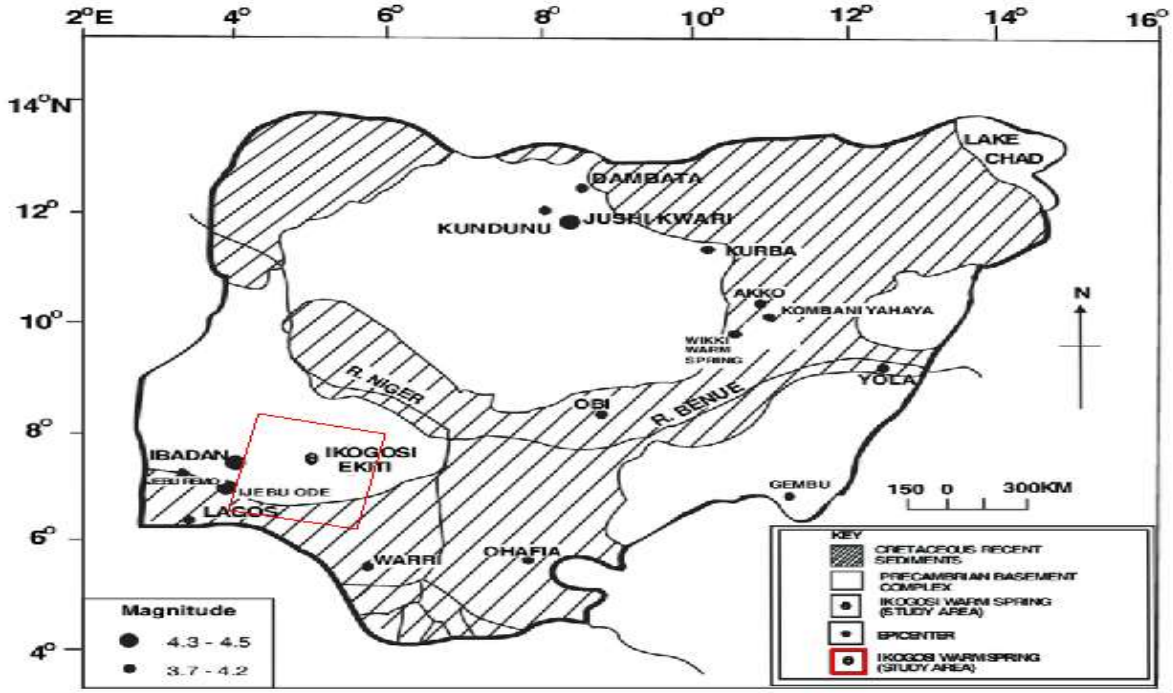

Figure 1: Geology map of the study area (modified after Adegbuyi and Abimbola, 1997)

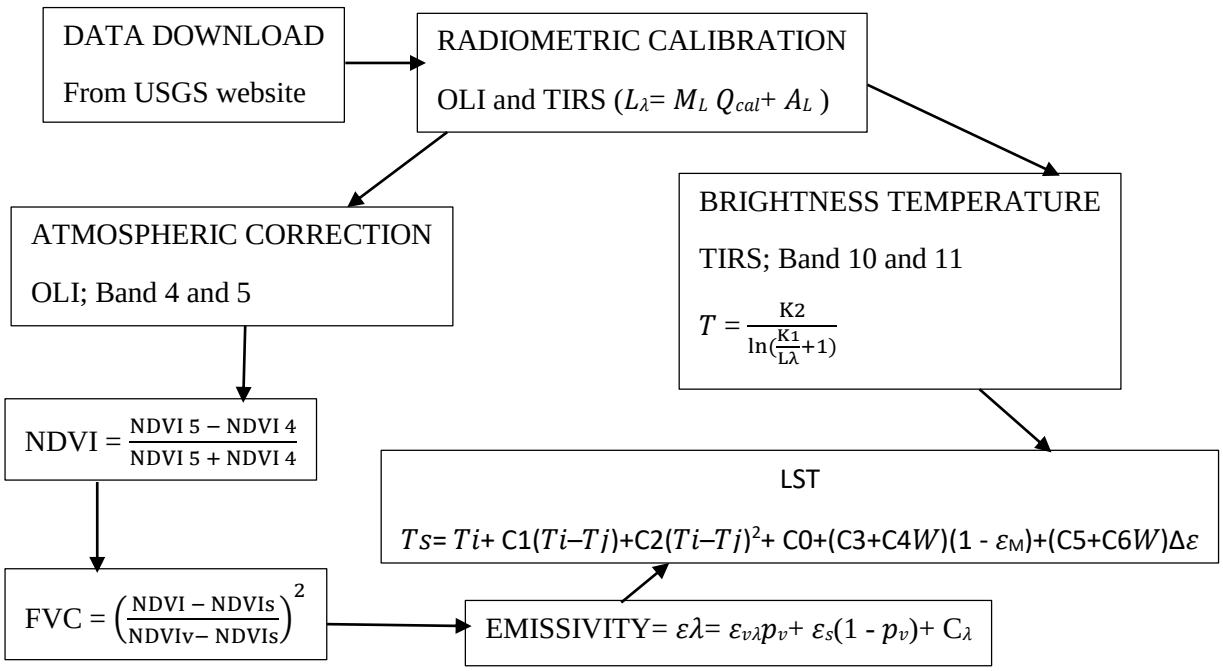

Figure 2: Chat illustrating a split-window procedure
OLI bands are largely contaminated by atmospheric conditions. Thus, atmospheric correction is required to retrieve the real surface parameters by removing the atmospheric effects, such as the absorption, upward emission, and scattering of the

radiation from the earth's surface for radiance. ENVI's Fast Line-of-sight Atmospheric Analysis of Spectral Hypercubes (FLAASH) module was used for atmospheric correction.

Table 1: LANDSAT 8 Radiance Scale Factors

BAND NUMBER	M_L	A_L
BAND 4	9.7443E-03	-48.72136
BAND5	5.9630E-03	-29.81504
BAND 10	3.3420E-04	0.10000
BAND 11	3.3420E-04	0.10000

FLAASH is a first-principles atmospheric correction modeling tool for retrieving spectral reflectance from hyperspectral radiance images. With FLAASH, atmospheric effects can accurately be compensated for. FLAASH corrects wavelengths in the visible through near-infrared and short-wave infrared regions, up to 3 µm. (For thermal regions, use the **Basic Tools - Preprocessing - Calibration Utilities - Thermal Atmospheric Correction** menu option.) Unlike many other atmospheric correction programs that interpolate radiation transfer properties from a pre-calculated database of modeling results, FLAASH incorporates the MODTRAN4 radiation transfer code.

FLAASH starts from a standard equation for spectral radiance at a sensor pixel, *L*, that applies to the solar wavelength range (assuming thermal emission is negligible) and flat, Lambertian materials or their equivalents. The equation is as follows:

$$L = \left(\frac{A\rho}{1-\rho_e S}\right) + \left(\frac{B\rho_e}{1-\rho_e S}\right) + L_a \qquad 2$$

where:

ρ is the pixel surface reflectance

ρ_e is an average surface reflectance for the pixel and a surrounding region

S is the spherical albedo of the atmosphere

L_a is the radiance backscattered by the atmosphere

A and B are coefficients that depend on atmospheric and geometric conditions but not on the surface.

The solution of the method involves computing a spatially averaged radiance image *Le*, from which the spatially averaged reflectance ρ_e is estimated using the approximate equation:

$$L_e \approx \left(\frac{(A+B)\rho_e}{1-\rho_e S}\right) + L_a \qquad 3$$

Atmospherically corrected OLI band 4 (red) and 5 (near-infrared) were layer stacked and NDVI was calculated using the Algorithm shown in equation 4. This data was used for input to derive fractional vegetation cover.

$$NDVI = \frac{\text{NDVI 5} - \text{NDVI 4}}{\text{NDVI 5} + \text{NDVI 4}} \qquad 4$$

Fractional vegetation cover, the percentage of vegetation occupying the ground area in vertical projection per unit area, is an important parameter in the $NDVI^{THM}$ method in emissivity study. The proportion of vegetation cover, Pv, for each pixel through satellite data is calculated using the following formula (Carlson and Ripley, 1997; Sobrino and Raissouni, 2000).

$$Pv = \left(\frac{\text{NDVI} - \text{NDVIs}}{\text{NDVIv} - \text{NDVIs}}\right)^2 \qquad 5$$

where NDVIv and NDVIs represent the NDVI of vegetation and soil, respectively. Over particular areas, NDVIv and NDVIs values were extracted from the NDVI histogram.

For those pixels composed of soil and vegetation (mixed pixels, NDVIs = NDVI = NDVIv), the method uses the following simplified equation 6 in this study.

$$\varepsilon_\lambda = \varepsilon_{v\lambda} P_v + \varepsilon_{s\lambda}(1 - P_V) + C_\lambda \qquad 6$$

where $\varepsilon_{s\lambda}$ and $\varepsilon_{v\lambda}$ are, respectively, the soil and vegetation emissivity, *C* is a term which considers the mean cavity effect due to surface roughness (*C* = 0 for flat surfaces). Using the geometrical model proposed by Sobrino *et al*., (2008). The cavity term for a mixed area like the study area is given by:

$$C_\lambda = (1 - \varepsilon_S)\varepsilon_{v\lambda} * F(1 - P_V) \qquad 7$$

Where C_λ is the contribution of multiple scattering caused by the internal geometric structure of the pixel for specific bands. F' is a geometrical factor ranging from zero to one, depending on the geometrical distribution of the surface. Since *F'* cannot be estimated from VNIR/TIR remote sensing data, a mean value is generally chosen (Sobrino and Raissouni, 2000). The mean value, assuming different geometrical distributions, is 0.55. The emissivity of soil and vegetative values for bands 10 and 11 of the corresponding bands are obtained from table 2 Jimenez-Munoz *et al*., (2014). After generating the cavity effect for bands 10 and 11, the mean cavity was obtained for each of the bands from the cavity histogram. Its result is used for input to calculate Emissivity.

Table 2: Emissivity value of vegetation and soil

Emissivity	Band 10	Band 11
Es	0.971	0.977
Ev	0.987	0.989

LSE measures the inherent characteristic of the earth's surface. LSE measures the earth's ability to convert thermal or heat energy into radiant energy. LSE estimation required emissivity of soil and vegetation of both Band 10 and 11 which are given in table 3.3. After generating LSE for both bands of TIR, the mean and difference of LSE values for the study area were obtained from equations 16 and 17 respectively (Sobrino et al., 2008). The data sets for mean and difference of LSE are very important parameters to calculate LST.

$\varepsilon_M = \frac{\varepsilon_{10}+\varepsilon_{11}}{2}$ 8

$\Delta\varepsilon = \varepsilon_{10} + \varepsilon_{11}$ 9

where ε_M is mean LSE, $\Delta\varepsilon$ is LSE difference and ε_{10} and ε_{11} are LSE of band 10 and 11

Satellite TIRS sensors measure TOA radiances, which were then converted to TOA brightness temperatures using Planck's equation, this procedure has been explained by Bello *et al.* (2020).

Split Window (SW) Algorithm was used to compute the land surface temperature of the area. The SW technique uses two TIR bands typically located in the atmospheric window between 10 and 12 μm. The basis of the technique is that the radiance attenuation for atmospheric absorption is proportional to the radiance difference of simultaneous measurements at two different wavelengths, each of them being subject to different amounts of atmospheric absorption. The SW algorithm adopted in this work is based on the mathematical structure proposed by (Jiménez-Munoz & Sobrino, 2003) and applied to different Earth Observation sensors (Sobrino *et al*., 2008).

The main advantages of this algorithm include the following: 1) It is a physics-based algorithm since it is obtained from the radiative transfer equation (RTE) applied to two different bands; 2) it takes into account both emissivity and water vapor effects; 3) it includes both LST and Sea surface temperature (SST) cases; and 4) it is operational (Sobrino *et al*., 2008).

LST was calculated by applying a structured mathematical algorithm using ENVI 5.1 band math tool, SW algorithm. It uses the brightness temperature of two bands of TIR, mean, and difference in land surface emissivity for estimating the LST of an area. The algorithm is shown in equation 10 below.

$T_S = T_i + C1(T_i - T_j) + C2(T_i - T_j)^2 + C0 + (C3 + C4W)(1 - \varepsilon_M) + (C5 + C6W)\Delta\varepsilon$ 10

where T_S is LST in kelvin, T_i and T_j are the at-sensor brightness temperatures at the SW bands i and j (in kelvin), ε_M is the mean emissivity, $\varepsilon_M = 0.5(\varepsilon_i + \varepsilon_j)$, $\Delta\varepsilon$ is the emissivity difference, $\Delta\varepsilon = (\varepsilon_i - \varepsilon_j)$. W is the total atmospheric water vapor content (in gcm^2), the value of water vapor (W) content was retrieved from MODIS. Its value is 4.12 g/cm^2. C0 - C6 is the value of the SW coefficient from Table 3.

Table 3: Split-Window Coefficient values (source: Skokovic *et al*., 2014).

Constant	Value
C0	-2.268
C1	1.378
C2	0.183
C3	54.3
C4	-2.238
C5	-129.2
C6	16.4

RESULT AND DISCUSSION

Result

The result of the red, near-infrared, and thermal infrared images of the bands 4, 5, and 10 and 11 (Table 4) respectively in which the DN were converted to the radiance are as shown in Figure 3 a and b and Figure 4a and b.

Table 4: Statistics of radiance for bands 4, 5, 10, and 11

Band	Minimum	Maximum	Mean	Standard Deviation
4	0.0	544.5	184.113158	132.184841
5	0.0	360.9	130.940379	89.375451
10	0.1	8.9	4.505154	2.994511
11	0.1	7.702255	4.228131	2.782075

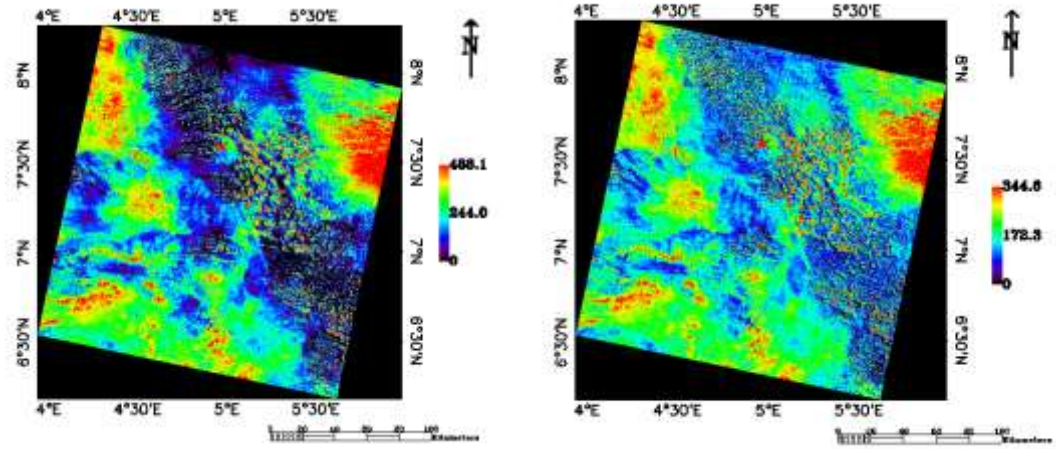

Figure 3 a & b: Radiance maps of the study area for bands 4 and 5, the point mark X represents Ikogosi warm spring.

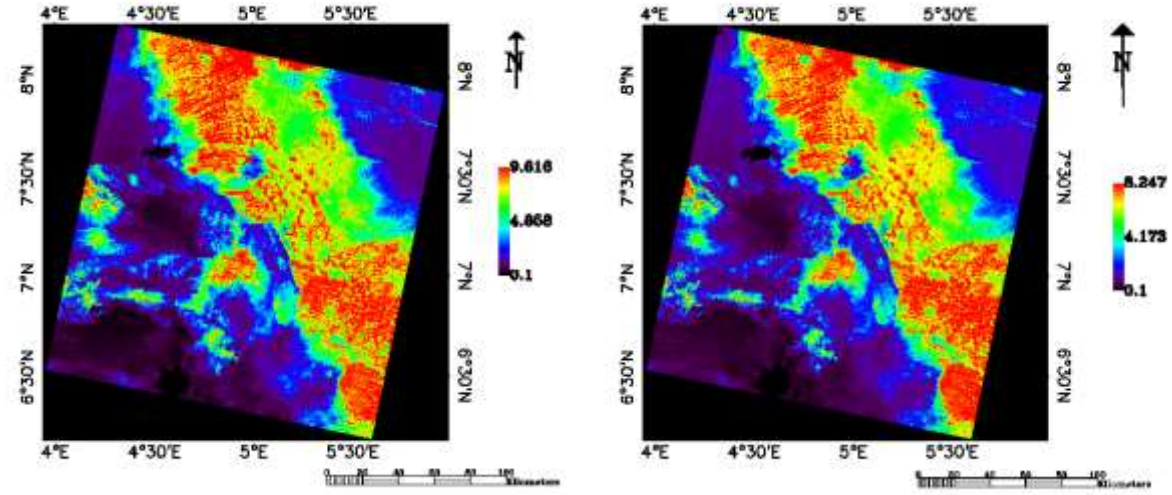

Figure 4 a & b: Radiance maps of the study area for bands 10 and 11, the point mark X represents Ikogosi warm spring.

From FLAASH model, which is used to reduce the atmospheric effect on the Landsat 8 data of the fourth band (red band) and fifth band (near-infrared band) bands, the reflectance was computed. The FLAASH reflectance output is between a negative value and over 10,000 (see table 5), but ideally, reflectance is between 0 and 1.

The expression below was inserted into the band math tool of ENVI to recompute the reflectance to range between 0 and 1:
(b1 le 0)*0+(b1 ge 10000)*1+(b1 gt 0 and b1lt10000)*float(b1)/10000

This implies; reflectance value less than or equal to 0 should be computed as 0, reflectance value greater than or equal to 10,000 be computed 1, and reflectance value between greater than 0 and greater than 10,000 are multiply by the ratio of reflectance and 10,000. The output of the rescaled reflectance for bands 4 and 5 are as shown in figure 5 a and b below respectively.

The computed reflectance for band 4 ranges from 0.000000 to 0.0115900 with a mean of 0.010892 and standard deviation of 0.015764. The reflectance of band 5 ranges from 0.000000 to 0.137200 with a mean of 0.030938 and a standard deviation of 0.023809. Reflection from the soil is high and produces low values of NIR and high values in the red band.

Table 5: Statistics of Reflectance for bands 4 and 5 from FLAASH algorithm

Band	Minimum	Maximum	Mean	SD
Band 4	-1843	14107	4546.811163	3287.707037
Band 5	0	14166	5047.453583	3447.851438

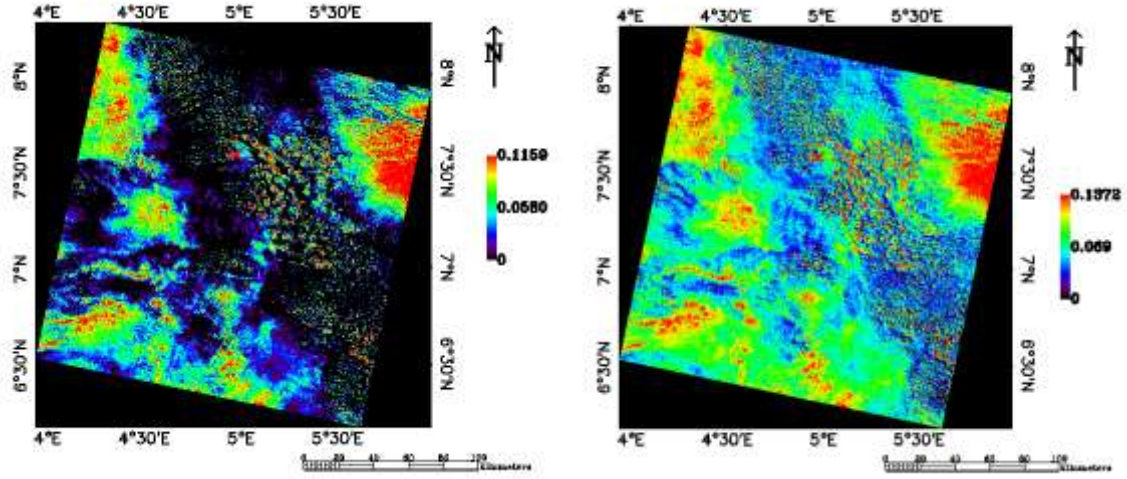

Figure 5 a &b: Rescaled reflectance for bands 4 and 5, the point mark X represents Ikogosi warm spring.

The result of the NDVI computed as shown in figure 6. From the histogram of NVDI (table 6) output, the lowest positive value of the study area are less vegetated soils, with the least number of point is 0.066667 (NDVIs). The highest value with the highest number of points 0.992157 is the highly vegetated areas (NDVIv). The extracted values are necessary input to derive FVC. The output value of computed NDVI ranged between 0.000000 and 1.000000 with a mean of 0.451884 and a standard deviation of 0.394688.

Table 6: NDVI histogram values for the study are

Band	**Minimum**	**Maximum**	**Mean**	**SD**	Approximate NDVIs	**Approximate NDVIv**
Band 1	0.000000	1.000000	0.451884	0.394688	0.066667	0.992157

The required NDVIs were inputted to yield the fractional vegetation cover of the study area. It represents the area in terms of percentage in the vertical projection of vegetation per unit area. The cavity term for a mixed area (C_λ) is the contribution of multiple scattering caused by the internal geometric structure of the pixel for specific bands, which takes into account the mean cavity effect due to the surface roughness. The estimated cavity effect for the mixed area and the near-nadir view is listed in table 6 below. The output of fractional cover was used to determine the emissivity of the study area.

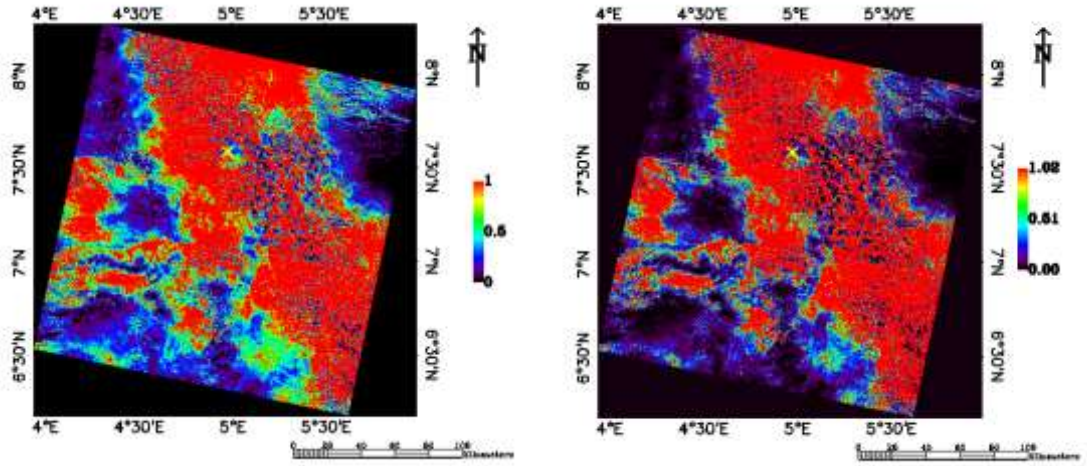

Figure 6:a) NDVI map of the study area, b) the percentage of the vertical projection of vegetation canopy map of the study area. The point mark X represents Ikogosi warm spring.

Table 7: Cavity effect Value of band 10 and 11

Band	**Minimum**	**Maximum**	**Mean**
Band 10	0.000	0.016	0.011
Band 11	0.000	0.013	0.009

Mean of Land Surface Emissivity was created using the NDVI threshold technique (Figure 7 a). The difference of LSE was calculated which is one of the important parameters to obtain LST using the SW algorithm. The emissivity was compared to the elevation distribution and geological units of the study area (Figures 7 a and b).
The computed LSE ranged between 0.987998 and 0.988127 with a mean of 0.988082.

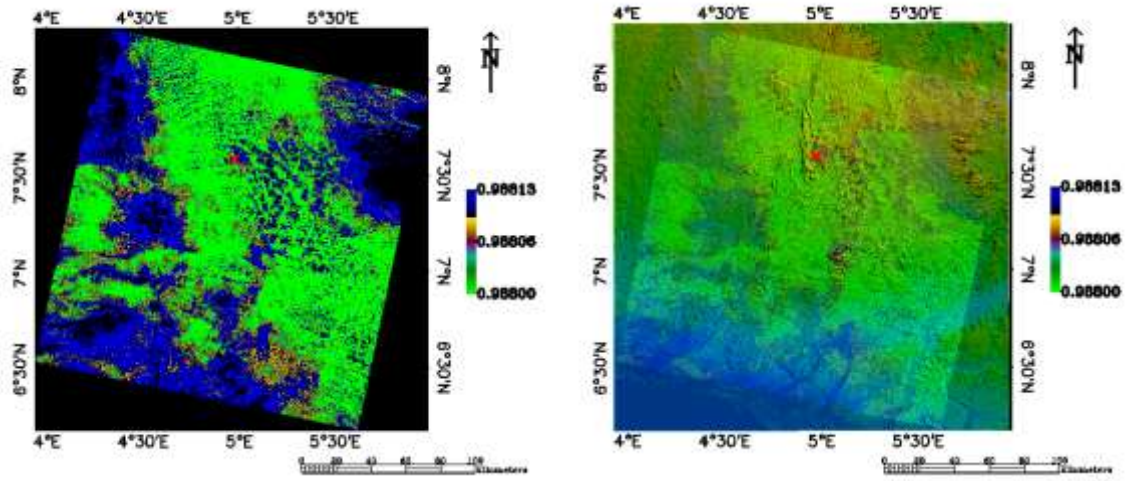

Figure 7 a & b: a) Mean of Land surface emissivity map of study area. B) an overlay of the mean of Land surface emissivity map on DEM map, the point mark X represents Ikogosi warm spring.

The result of at-satellite temperature ranges from -125.48291 °C to 22.194275 °C for band 10. The value ranges from -131.329376 °C to 17.142487 °C for band 11. They were used to compute the brightness temperature for band 10 ranges from -125.48291 °C to 27.137115 °C and the brightness temperature for band 11 ranges from -131.329376 °C to 21.195160 °C. Figures 8 a and b are the maps of the brightness

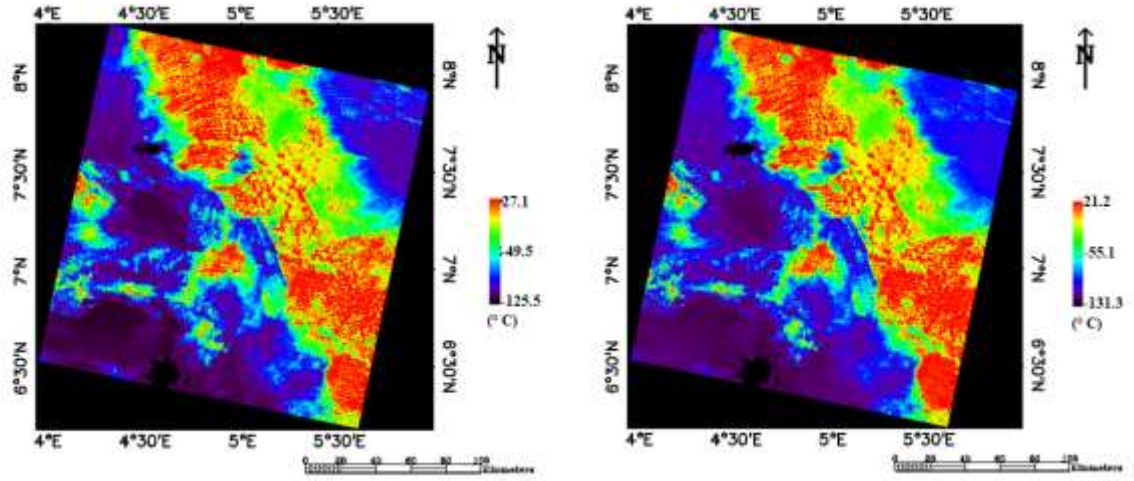

Figure 8 a & b: Top of Atmosphere Brightness Temperature map for bands 10 and 11, the point mark X represents Ikogosi warm spring.

The LST of the study area (Figure 9 a) was computed using mean LSE, brightness temperature and emissivity difference of band 10 and 11 of TIR. LST output portrayed that it varied from -12 °C to 59 °C with a mean of 5.518003 °C. The temperature distribution was reclassified to map out regions with highest temperature range (Figure 9 b).

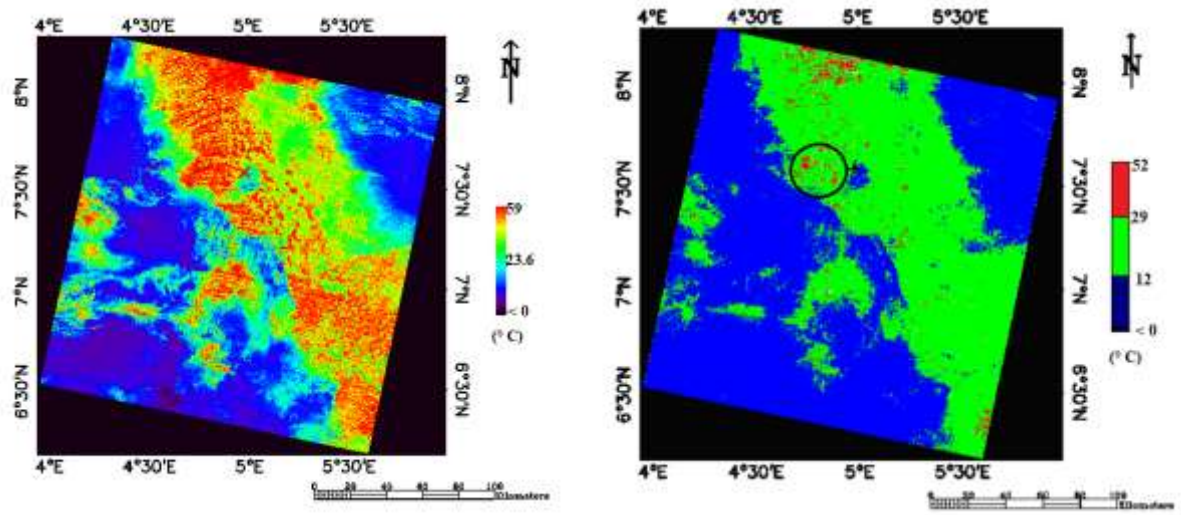

Figure 9 a&b: Land Surface Temperature distribution and the reclassified LST maps of the study area. The point mark X

Discussion

In this study, the region around Ikogosi warm spring (IWS) is made up of high radiance in bands 4, 5, 10, and 11 (Figures 3 a & b and 4 a&b), low reflectance in band 4 but moderate reflectance in band 5 (Figures 5 a and b). The NDVI was used to assess the impact of geothermal energy on the vegetation in the study area. The result around IWS suggests high vegetation, though the eastern vicinity (which is around the meeting point of the springs) is low due to the water body and activities of tourists (see figure 6 a). The is a reflection of the situation on the ground.

Similar behaviour is observed in the result of the vegetation cover of the study area. The IWS is characterized by a high percentage, about 100 %, of the vertical projection of vegetation canopy and the eastern vicinity, which is sharply low, far less than 50% (see figure 6 b). The calculated mean LSE around the IWS is observed to be moderate while the eastern vicinity is very high (see figure 7a) and the LSE appears not to be influenced by elevation as shown in figure 6 b, and highly vegetated regions are characterized by low LSE. (Figure 6a and 7 a)

The top of the atmosphere brightness around IWS is a bit high, about 10 °C, in band 10 and less than 10 °C in band 11 (see figure 8 a and b). Highly vegetated regions are of high brightness temperature in both bands. The brightness temperature of the study area and the surface temperature map of Nigeria within the study area concordantly show temperature drop towards the southwest direction (see Bello *et al.,* 2020). The trend of the LST distribution map shows temperature drop towards the southwest direction (Figure 9 a). The LST result around the IWS is about 35 °C as shown in figure 8a. The reclassification of the LST revealed two hot spot zones; NW of IWS and west of IWS, which are about 52 °C as compared to around IWS with a temperature of about 29 °C. It can then be suggested that the hot spot regions west of IWS are contributing to the high temperature of the spring due to its proximity and its direction to IWS being concordant to the direction of IWS to the meeting point of the springs.

CONCLUSIONS AND RECOMMENDATIONS

The computation of the LST from the Landsat8 data revealed that the warm spring is situated around a region with high land surface temperature (about 29 °C) which is an indication of a geothermal reservoir. The map of the reclassified LST reveals two hot spot zones. The hot spots zone west of IWS is believed to be the heat source of IWS as it has high LST, and closer to IWS The hot spots zone NW of IWS shows an indication of a viable geothermal resource, high LST.

It is recommended, based on findings from this work, that the core drilling of identified regions of thermal anomalies be carried out to assess the temperature variation with depth and it is also suggested that the identified regions should be protected by the authorities.

REFERENCE

Abraham, E.M., Lawal, K. M., Ekwe, A. C., Alile, O., Murana, K. A., and Lawal, A. A. (2014). Spectral analysis of aeromagnetic data for geothermal energy investigation of Ikogosi Warm Spring - Ekiti State, southwestern Nigeria. *Geothermal Energy*, *2*(1), 1–21. https://doi.org/10.1186/s40517-014-0006-0

Adegbuyi, O. & Abimbola, A.F., 1997. Energy resource potential of Ikogosi Warm Spring Area, Ekiti State, Southwestern Nigeria, African Journal of Science, 1(2), 111–117

Adegbuyi, O., Ajayi, O.S., and Odeyemi, I. B. (1996). Prospects of hot-dry-rock (HDR) geothermal energy spectrophotoresource around the Ikogosi warm spring in Ekiti state, Nigeria. *Nigerian Journal of Renewable Energy*, *4*, 58–64.

Bello, Y.A., Lawal, K.M., Dewu, B.B.M. and Ikpkonte, A.E. (2020) Use of at-satelite temperature for geothermal investigation in Ikogosi. *FUDMA Journal of Sciences,* 4(1): 389 – 394.

Carlson, T.N., and Ripley, D.A. (1997). On the relation between NDVI, fractional vegetation cover, and leaf area index. *Remote Sensing of Environment*, *62*(3), 241–252. https://doi.org/10.1016/S0034-4257(97)00104-1

Chan, H., Chang, C. and Dao, P.D. (2018). Geothermal anomaly mapping using Landsat ETM+ Data in Ilan Plain, Plain, Northeastern Taiwan. *Elsevier, Pure and Applied Geophysics*, 175: 303 – 323.

Heasler, H., Jaworowski, C., and Foley, D. (2009). Geothermal systems and monitoring hydrothermal features. *Geological Monitoring*, 105 - 140.

Jiménez-Munoz, J.C. and Sobrino, J.A. (2003). A generalized single-channel method for retrieving land surface temperature from remote sensing data. *Journal of Geophysical Research D: Atmospheres*, *108*(22). https://doi.org/10.1029/2003jd003480

Jimenez-Munoz, J.C., Sobrino, J.A., Skokovic, D., Mattar, C. and Cristobal, J. (2014). Land surface temperature retrieval methods from landsat-8 thermal infrared sensor data. *IEEE Geoscience and Remote Sensing Letters*, *11*(10), 1840–1843. https://doi.org/10.1109/LGRS.2014.2312032

Nicholson, K. (1993). Geothermal Fluids: Chemistry and exploration techniques. Springer

Norman, J. M., and Becker, F., 1995. Terminology in thermal infrared remote sensing of natural surfaces. *Remote Sensing Reviews*, 12: 159 – 173.

Ojo, J.S., Olorunfemi, M.O. and Falebita, D.E. (2011). An appraisal of the geologic structure beneath the Ikogosi warm spring in South-Western Nigeria using integrated surface geophysical methods. In *Earth Sciences Research Journal* (Vol. 15, Issue 1, pp. 27–34).

Olorunfemi, M.O., Adepelumi, A.A., Falebita, D.E. & Alao, O.A., 2011. Crustal thermal regime of Ikogosi warm spring, Nigeria inferred from aeromagnetic data, Arabian Journal of Geosciences, doi:10.1007/s12517011-0486-1.

Skokovic, D., Sobrino, J. a., Jiménez Muñoz, J. C., Soria, G., Julien, Y., Mattar, C., and Cristóbal, J. (2014). Calibration and Validation of land surface temperature for Landsat8-TIRS sensor TIRS LANDSAT-8 CHARACTERISTICS. *Land Product Validation and Evolution ESA/ESRIN*, 27. https://doi.org/10.1063/1.452862

Sobrino, J.A. and Raissouni, N. (2000). Toward remote sensing methods for land cover dynamic monitoring: Application to Morocco. *International Journal of Remote Sensing*, *21*(2), 353–366. https://doi.org/10.1080/014311600210876

Sobrino, José A., Jiménez-Muñoz, J. C., Sòria, G., Romaguera, M., Guanter, L., Moreno, J., Plaza, A., and Martínez, P. (2008). Land surface emissivity retrieval from different VNIR and TIR sensors. *IEEE Transactions on Geoscience and Remote Sensing*, *46*(2), 316–327. https://doi.org/10.1109/TGRS.2007.904834